Functional Changes Within the Rod Inner Segment Ellipsoid in Wildtype Mice: An Optical Coherence Tomography and Electron Microscopy Study

Bruce A. Berkowitz,[1] Robert H. Podolsky,[2] Karen Lins Childers,[3] Tom Burgoyne,[4] Giulia De Rossi,[4] Haohua Qian,[5] Robin Roberts,[1] Ryan Katz,[1] Rida Waseem,[1] and Cole Goodman[1]

[1]Department of Ophthalmology, Visual and Anatomical Sciences, Wayne State University School of Medicine, Detroit, Michigan, United States
[2]Biostatistics and Study Methodology, Children's National Hospital, Silver Spring, Maryland, United States
[3]Beaumont Research Institute, Beaumont Health, Royal Oak, Michigan, Unites States
[4]UCL Institute of Ophthalmology, University College London, London, United Kingdom
[5]Visual Function Core, National Eye Institute, National Institutes of Health, Bethesda, Maryland, Unites States

Correspondence: Bruce A. Berkowitz, Wayne State University School of Medicine, 540 E. Canfield, Detroit, MI 48201, USA; baberko@med.wayne.edu.

Received: February 9, 2022
Accepted: June 19, 2022
Published: July 11, 2022

Citation: Berkowitz BA, Podolsky RH, Childers KL, et al. Functional changes within the rod inner segment ellipsoid in wildtype mice: An optical coherence tomography and electron microscopy study. *Invest Ophthalmol Vis Sci.* 2022;63(8):8. https://doi.org/10.1167/iovs.63.8.8

Purpose. To test the hypothesis that changing energy needs alter mitochondria distribution within the rod inner segment ellipsoid.

Methods. In mice with relatively smaller (C57BL/6J [B6J]) or greater (129S6/ev [S6]) retina mitochondria maximum reserve capacity, the profile shape of the rod inner segment ellipsoid zone (ISez) was measured with optical coherence tomography (OCT) under higher (dark) or lower (light) energy demand conditions. ISez profile shape was characterized using an unbiased ellipse descriptor (minor/major aspect ratio). Other bioenergy indexes evaluated include the external limiting membrane–retinal pigment epithelium (ELM-RPE) thickness and the magnitude of the signal intensity of a hyporeflective band located between the photoreceptor tips and apical RPE. The spatial distribution of rod ellipsoid mitochondria were also examined with electron microscopy.

Results. In B6J mice, darkness produced a greater ISez aspect ratio, thinner ELM-RPE, and a smaller hyporeflective band intensity than in light. In S6 mice, dark and light ISez aspect ratio values were not different and were greater than in light-adapted B6J mice; dark-adapted S6 mice showed smaller ELM-RPE thinning versus light, and negligible hyporeflective band intensity in the light. In B6J mice, mitochondria number in light increased in the distal inner segment ellipsoid and decreased proximally. In S6 mice, mitochondria number in the inner segment ellipsoid were not different between light and dark, and were greater than in B6J mice.

Conclusions. These data raise the possibility that rod mitochondria activity in mice can be noninvasively evaluated based on the ISez profile shape, a new OCT index that complements OCT energy biomarkers measured outside of the ISez region.

Keywords: photoreceptor, OCT, energy

Dysfunction of mitochondria and their linked/downstream processes within the rod cell, collectively referred to herein as the rod energy-landscape, are thought to be a common pathogenic condition underlying visual performance declines during physiological aging and in sight-threatening neurodegenerative diseases.[1–16] Yet few translational imaging biomarkers can evaluate the trajectory of early rod energy-landscape changes. The availability of noninvasive imaging indexes is desirable to enable the translation of pro-survival treatments from experimental models into patients helping to decrease the risk of sight-threatening disease.

To address this problem, we have developed imaging biomarkers that are sensitive to changes in the rod energy-landscape during, for example, dark (higher energy demand) and light (lower energy demand) adaptation.[17–20] One example of a mitochondria-linked process is a dark-evoked pH-dependent thinning of the external limiting membrane-retinal pigment epithelium (ELM-RPE) region compared to that in light (more detail in discussion); this thinning is measurable with microelectrodes + an extracellular tracer, diffusion magnetic resonance imaging (MRI), and optical coherence tomography (OCT).[11,12,21–31] Oxidative stress can also be detected by QUench-assiSTed (QUEST) OCT based on the dark-light ELM-RPE thickness.[32] More recently, we showed that the magnitude of a hyporeflective band signal intensity located between photoreceptor tip and apical RPE layers is correlated with dark-light ELM-RPE changes in wild-type mice but is pH independent; this hyporeflective band is seen in humans, and work is ongoing to understand

what this band represents.[27,32–38] Dark-evoked thinning of ELM-RPE and reduction in magnitude of the hyporeflective band signal intensity observed between the photoreceptor tips and apical RPE have been measured in humans.[28,33]

ELM-RPE thickness and magnitude of the hyporeflective band signal intensity are indirect bioenergy indexes because both are spatially removed from the rod inner segment ellipsoid, a region that is ~75% full of mitochondria.[39–42] A more direct proxy of rod inner segment ellipsoid mitochondria and their activity is desirable. This seems possible because a hyperreflective outer retina immediately posterior to the ELM is readily identified and has been designated with common consensus as the inner segment ellipsoid zone (ISez).[39,40,43–46] However, different OCT-based approaches appear to come to a different anatomic interpretation regarding this hyperreflective band with some evidence supporting the inner segment/outer segment boundary and some the ellipsoid zone. Nonetheless, the OCT ISez band is an accepted biomarker of photoreceptor health whose absence, for example, is predictive of outer retina degeneration.[39,40,43–46]

To examine differences in the rod energy-landscape, we examined C57BL/6J (B6J) versus 129S6/ev (S6) mice in light and dark conditions. B6J mice show an 11% lower retinal mitochondria efficiency than S6 mice.[30,47] This strain difference is based on oxygen consumption rate measurements of freshly isolated retina.[30] Whole retinal mitochondria efficiency has a dominant contribution from rods, the most numerous cell type in the mouse retina.[29,30,33,48–51] Also, these two strains show light versus dark patterns in vivo in R1 MRI (a proxy for free radical production) in the ISez identified on OCT, outer retina water content (measured with MRI), and in ELM-RPE thickness and magnitude of the hyporeflective band signal intensity.[29,30,32,33] Furthermore, B6J and S6 mice show distinct patterns of sodium iodate-induced rod oxidative stress (measured with QUEST MRI), and severity of retinal degeneration following sodium iodate.[49] Intriguingly, B6J mice lack the mitochondria nicotinamide nucleotide transhydrogenase (*Nnt*) gene, a mutation not reported for S6 mice.[47] The absence of *Nnt* in B6J mice is expected to decrease ATP synthesis efficiency with perhaps a corresponding reduction in coordinated regulation of energy-dependent processes.[47] All available data support the notion that S6 mice have a relatively higher mitochondria activity than B6J mice and better regulation/coordination of associated events.[29,30,32,33,49]

In this study, we asked how light-scattering by mitochondria and their aggregates within the rod inner segment ellipsoid, which have been reported to spatially rearrange via fusion, fission, and translocation (key events involved with addressing bioenergetic demand), alter the ISez profile shape as measured by OCT.[40,52–55] In addition, an electron microscopy (EM) study was performed to determine how the number of mitochondria within distal, mid, and proximal thirds of rod inner segment ellipsoid change under light and dark conditions.

Methods

All mice were treated in accordance with the National Institutes of Health Guide for the Care and Use of Laboratory Animals, the Association for Research in Vision and Ophthalmology Statement for the Use of Animals in Ophthalmic and Vision Research, and with specific authorization by the Wayne State University Division of Laboratory Animal Resources Institutional Animal and Care Use Committee (IACUC). For the OCT studies performed at Wayne State University, 2 mo male and female C57BL/6J mice (B6J; n = 5 dark/sex, n = 5 light/sex; Jackson Laboratories, Bar Harbor, ME, USA), and male 129S6/ev mice (S6; n = 5 dark, n = 5 light; Taconic Laboratories, Rensselaer, NY, USA) were housed and maintained in 12-hour/12-hour light-dark cycle laboratory lighting. After scanning, mice were humanely euthanized by an overdose of ketamine/xylazine followed by cervical dislocation, per our Wayne State University Institutional Animal and Care Use Committee–approved protocol. Data were collected from the left eye.

For the transmission EM studies performed at the University College London, 2 mo male B6J or S6 mice were maintained in 12-hour/12-hour light-dark cycle laboratory lighting. The eyes used were from B6J mice killed by cervical dislocation in accordance with Home Office (United Kingdom) guidance rules under project licenses 70/8101 and 30/3268. The eyes used from S6 mice were similarly obtained and fixed at Wayne State University and then sent to University College London for analysis.

Optical Coherence Tomography

Using a cross-sectional design, two-month-old male and female B6J, and male S6 mice, were either dark-adapted overnight and room light-adapted (~1200 lux) for one hour the following day, or dark-adapted overnight and studied in the dark the following day. All groups were examined in the morning (i.e., before noon) using an Envisu UHR2210 OCT (Bioptigen, Inc., Morrisville, NC, USA). Mice were anesthetized only once with 100 mg/kg ketamine/6 mg/kg xylazine cocktail (Sigma-Aldrich, St. Louis, MO, USA). One percent atropine sulfate was used to dilate the iris, and Systane Ultra was used to lubricate the eyes. From the central retina, we collected radial volume scan with the following parameters: A-scans/B-scans = 1000 lines; B-scans/volume = 1000 scans; Frames/B-scan = 1 frame. One hundred images extracted from B scan numbers 450–549 (representing inferior-superior retina) were registered (in-house R script). Briefly, first-pass rigid body registration with RNiftyReg (function in R) is used to rotate the image and interpolate signal at each pixel. Next, non-rotational rigid-body approaches (at the level of a given row or column of pixels) are applied three times. The 100 images are finally compared visually as a final step before averaging. Inferior and superior retina (±350 to 624 µm from the optic nerve head) were separately analyzed for ISez profile shape (i.e., OCT intensity along the length of the ISez; ImageJ macro's [available upon request]).[56] The intensity values used to generate the ISez shape profile are obtained from a log-based image (default in the Bioptigen system). Using an empirically derived equation, we compared a small subset of images before and after converting them from log to linear values in a preliminary study.[40] Similar shapes and standard deviations were noted suggesting that ISez profile shape differences noted in the results would be detected with either output (data not shown). In brief, built-in functions within ImageJ were used to characterize the ISez profile shape after transformation into an equivalent ellipse with the same area, orientation, and centroid.[57] More specifically, the second-order moment of the shape profile allows us to compute an ellipse that has the same moment, orientation, and centroid as the profile shape. From this ellipse, a minor/major aspect ratio was calculated and used as an unbiased outcome index that analytically characterizes in a single value the ISez profile shape. The processing

Investigative Ophthalmology & Visual Science

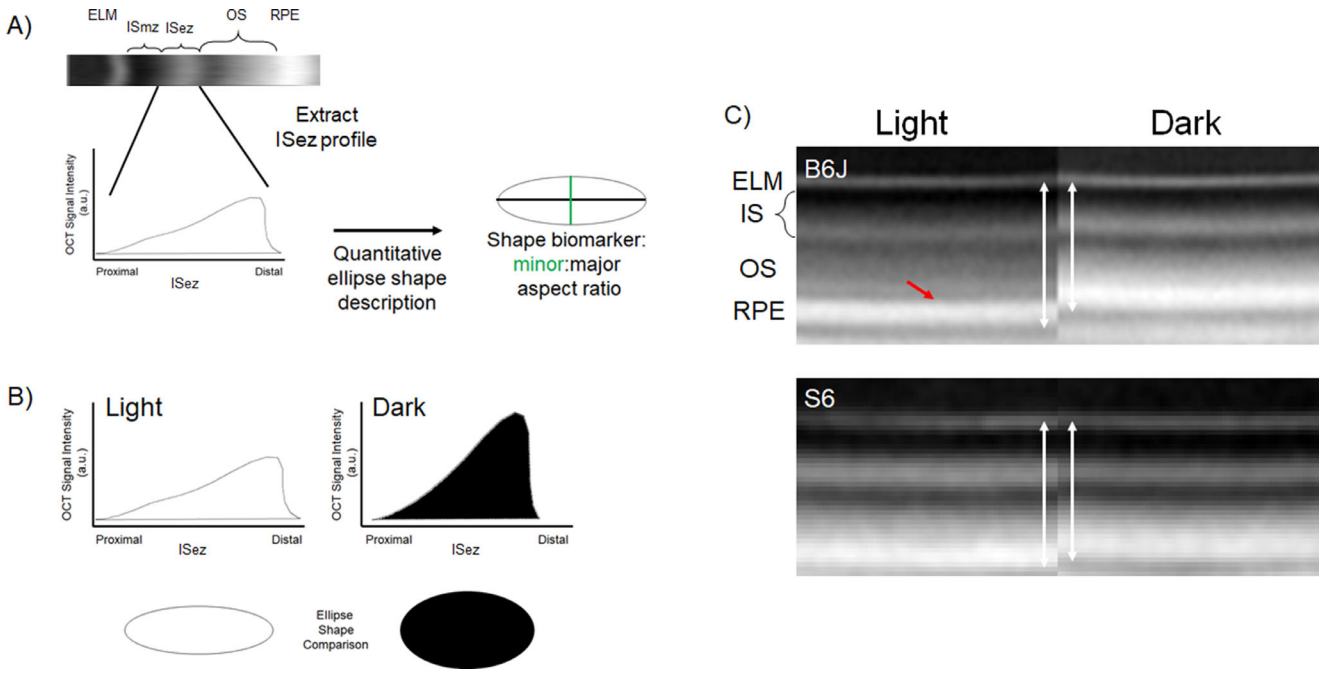

Figure 1. Illustration of the three functional OCT biomarkers studied. (**A**) The first biomarker is derived from the hyperreflective portion of the inner segment called the ellipsoid zone (ISez, consensus nomenclature) shown on a representative OCT of the outer retina of a B6J mouse.[46] The ISez is densely packed with light-scattering mitochondria; if the mitochondria change distribution or shape in response to various cellular energy needs, one expects the light-scattering pattern to change. The relatively hyporeflective myoid zone of the inner segment (i.e., the "ISmz") contains mostly ribosomes, endoplasmic reticulum, and Golgi bodies.[39,53] Other OCT landmarks shown are the ELM, outer segment (OS), and retinal pigment epithelium. From the B-scan we first extract the corresponding ISez profile. Mathematically, the second moment of this profile is described as an ellipse of the same area, centroid, and orientation as the profile (smaller right) to generate an output shape biomarker and minor/major aspect ratio; note here the light-dark ellipses have the same area scaling factor but that factor is reduced from that of the profiles for illustrations purposes. No baseline subtraction was performed. (**B**) Example of mean ISez profiles from light ($n = 5$) or dark ($n = 5$) male B6J mice illustrating the shape change on OCT (top row) and in corresponding ellipses (bottom row). Statistical analyses of the ISez aspect ratio values are shown in Figure 2. (**C**) Two other OCT-based rod energy-landscape biomarkers evaluated in this study are the ELM-RPE thickness (*white vertical double-headed arrows*) and magnitude of the hyporeflective band signal intensity (*red arrow*); example images from B6J (*top*) and S6 (*bottom*) are shown. Compared to the smaller energy demand condition of light, dark (higher energy condition) is associated with the ISez aspect ratio becoming rounder, the ELM-RPE region thinning, and a reduction in the magnitude of the hyporeflective band signal intensity.[33]

flow steps for generating the ISez aspect ratio are outlined in Figure 1A.

The other two biomarkers evaluated (i.e., ELM-RPE thickness and magnitude of the hyporeflective band signal intensity, illustrated in Fig. 1C) were generated from in-house R scripts that objectively extracted layer boundaries obtained after searching the space provided by a hand-drawn estimate ("seed boundaries"). The ELM and RPE are initially identified by local signal maxima and the R script determines the ELM-RPE thickness by calculating the distance from ELM to the basal side of the RPE at the level of Bruch's membrane.[57–59] The magnitude of the hyporeflective band signal intensity is calculated as previously described by analyzing profile contours spanning the RPE and outer segment tips: A straight line is drawn between the RPE and the outer segment tip portions of the profile (intersecting only one point on each side of hyporeflective band), and the largest departure from that line is the magnitude of the hyporeflective band signal intensity; the magnitude of this signal "dip" is presented herein.[29,33,60]

Transmission Electron Microscopy

S6 ($n = 3$) or B6J ($n = 3$) mice were dark adapted overnight, and S6 ($n = 3$) or B6J ($n = 3$) followed the normal light/dark cycle (light). The following morning, in the dark, under red light or after a one-hour light adaptation, mouse eyes were removed and placed straight into fixative (2% paraformaldehyde/2% glutaraldehyde in 0.15 M cacodylate buffer) for one hour at room temperature. After this time, eyes were washed in 0.1M cacodylate buffer, the cornea was carefully cut away, and the lens was removed before fixing for a further hour at room temperature. All B6J mouse eyes were prepared for transmission electron microscopy as follows.[61] Eyes were incubated in undiluted UA-Zero (Agar) for two hours after incubation with 1% osmium tetroxide/1% potassium ferrocyanide to provide en bloc staining. All S6 eyes were prepared using a similar method that included additional en bloc staining steps. The reason for the variation in staining method was that these sample were originally prepared with the aim to use them for 3D serial block face scanning microscopy that requires high sample contrast. This includes an additional osmium tetroxide step and en bloc staining with thiocarbohydrazide solution, uranyl acetate (instead of UA-zero) and lead citrate (https://ncmir.ucsd.edu/sbem-protocol). This variation in sample staining should not affect positioning of organelles as has been shown in studies using correlative light electron microscopy, where fluorescently labeled organelles remain in the same position in EM samples prepared using the same high-contrasted method.[62,63] For all samples, ~100 nm–thick sections were cut and imaged using a JEOL 1400+ transmission EM equipped with a Gatan Orius SC1000B charge-coupled device camera. For each strain, 15 inner segments

were examined from dark-adapted ($n = 3$) and one-hour light-adapted ($n = 3$) mice. Measurements of the mitochondria position within inner segments were performed in ImageJ using a macro written to divide only the ISez into three equal regions (distal, mid, and proximal).[56]

Statistical Analysis

Data are presented as mean and 95% confidence intervals. A significance level of 0.05 was used for all tests. For each mouse, we first averaged ELM-RPE thickness measured ± 350 to 624 µm from the optic nerve head. We used the same modeling strategy for all outcomes (ISez aspect ratio shape, ELM-RPE thickness, and magnitude of the hyporeflective band signal intensity). A linear mixed model was used that included the fixed effects of light/dark, side (inferior vs. superior), group (B6J male, B6J female, and S6 male), all interactions, and a random intercept for mouse within light versus dark (i.e., the light condition) and group. We evaluated whether residual variances depended on light condition or group using the Akaike and Schwarz Bayesian information criteria (AIC and BIC). None of the outcomes showed a decrease in either AIC or BIC greater than 10 leading us to assume the residual variance was constant across both light condition and group. We used Kenward-Roger degrees of freedom in testing all fixed effects for these models. These models were fit using Proc Mixed in SAS/STAT v15.1 (2016).

The number of mitochondria within a region for the electron microscopy data was analyzed using a generalized linear mixed model that included the fixed effects of light condition, strain (B6J vs. S6), region and the light condition/strain/region interaction, and random intercepts for mouse within light condition/strain, image within mouse/light condition/strain, and inner segment ellipsoid within image/mouse/light condition/strain. The model used a log link and the Poisson distribution. The log of the mitochondrial width within strain was analyzed using a linear mixed model that included the fixed effects of light condition, strain and the light condition/strain interaction, random intercepts for mouse within light condition/strain, and image within mouse/light condition/strain. For all models, higher-order interactions were evaluated first and removed if not significant until all interactions included in the model were either significant or removed from the model. Linear contrasts were used to compare groups.

Results

Rod ISez Aspect Ratio

A representative example from light- or dark-adapted B6J mice illustrates the visibly apparent change in rod ISez

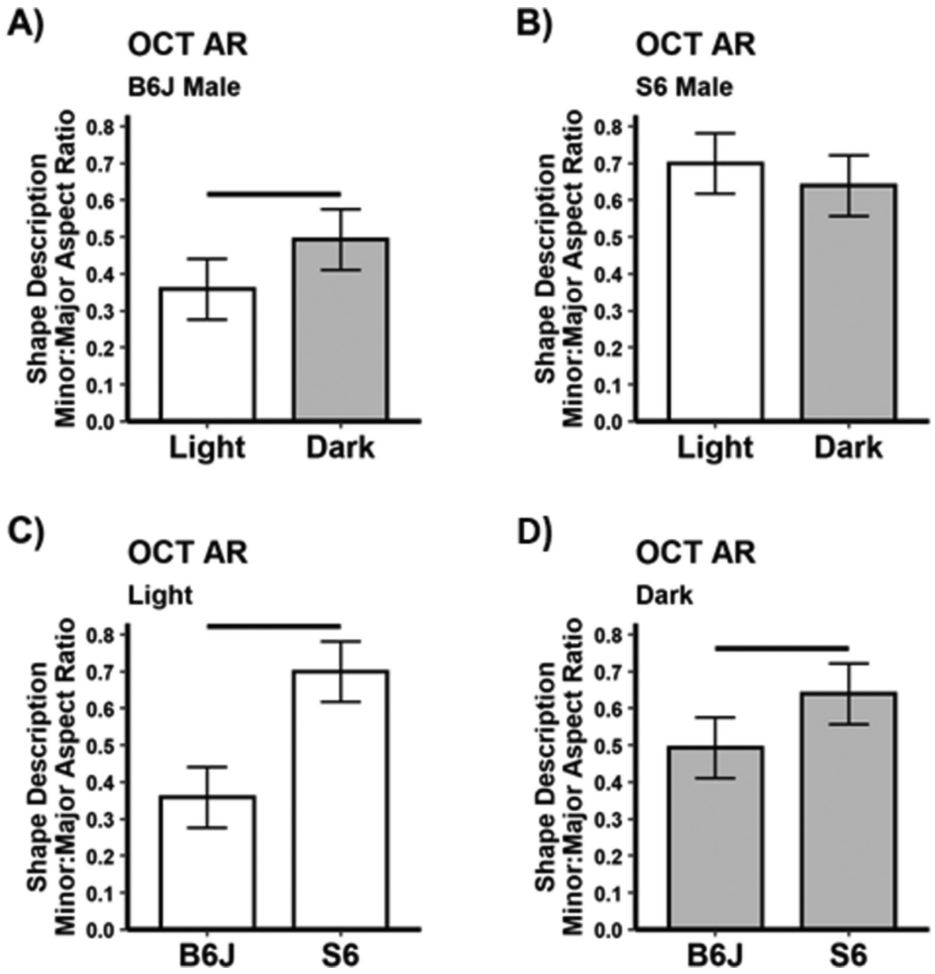

Figure 2. Higher energy demands in the dark are associated with a greater (i.e., rounder) ISez aspect ratio and lower energy demands in the light with a smaller (i.e., more elliptical) ISez aspect ratio in B6J versus S6 mice. Summary of (**A**) B6J and (**B**) S6 ISez for light versus dark male mice on the superior retina (inferior results are shown in Supplementary Figure S1). Comparisons of B6J and S6 ISez for (**C**) light and (**D**) dark mice. All groups $n = 5$, mean ± 95% confidence interval. *Black horizontal bar*: $P < 0.05$.

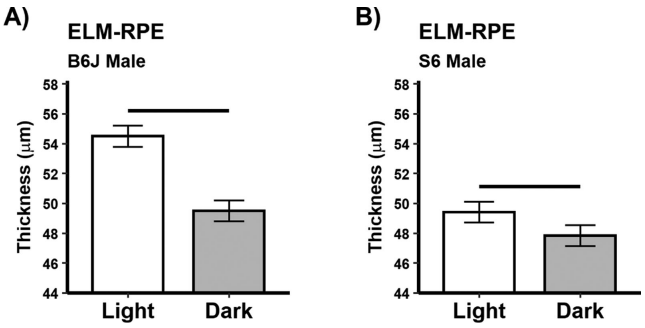

Figure 3. Greater energy demands in the dark are associated with a thinner ELM-RPE compared to that in the light. Summary of (**A**) B6J and B) S6 ELM-RPE thickness for light versus dark male mice on the superior retina (inferior results are shown in Supplementary Figure S2). All groups $n = 5$, mean ± 95% confidence interval. *Black horizontal bar*: $P < 0.05$.

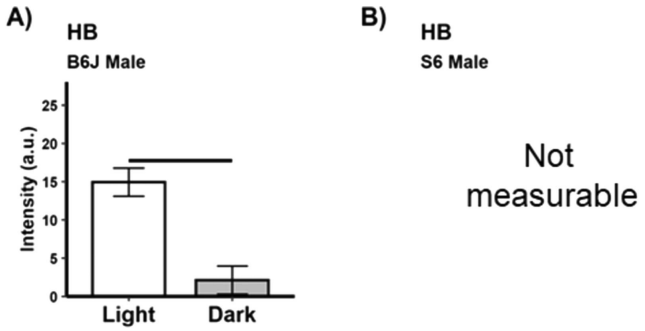

Figure 4. Greater energy demands in the dark are associated with a smaller magnitude of the hyporeflective band signal intensity than in the light.[17–20] Summary of (**A**) magnitude of the hyporeflective band signal intensity for light versus dark in male B6J mice on the superior retina (inferior results are shown in Supplementary Figure S3). All groups $n = 5$, mean ± 95% confidence interval. *Black horizontal bar*: $P < 0.05$. (**B**) No measurable magnitude of the hyporeflective band signal intensity was noted for S6 mice, consistent with a higher mitochondria efficiency in this strain versus that in B6J mice.[30]

profile shape and corresponding ellipses (Fig. 1B). Analytically, the difference in ISez aspect ratio is significant ($P < 0.05$) in light and dark male B6J mice on the superior (Fig. 2) and inferior (Supplementary Fig. S1) retina; similar results were also found in female B6J mice (Supplementary Fig. S1). In contrast, male S6 mice show neither inferior nor superior rod ISez aspect ratio light versus dark differences (Fig. 2). In light-adapted male B6J and S6 mice, the ISez aspect ratio were different on superior and inferior sides ($P < 0.05$); however, in dark-adapted mice, a strain difference ($P < 0.05$) was found on the superior side (Fig. 2), but not the inferior side (Supplementary Fig. S1).

Rod ELM-RPE Thickness and Magnitude of the Hyporeflective Band Signal Intensity

As expected, dark-adapted male B6J mice showed significant ($P < 0.05$) thinning of superior and inferior central ELM-RPE (Fig. 3, previously confirmed with microstructure measurements such as histology and diffusion MRI.[22,27,64,65]), and a smaller magnitude of the hyporeflective band signal intensity (Fig. 4) compared to that than in the light; similar results were also found in female B6J mice (Supplementary Fig. S2).[21] Although male S6 mice showed light versus dark thinning of the ELM-RPE, the extent of thinning was, as expected, significantly less than that for B6J mice (Fig. 3).[30] In male S6 mice, no discernable "dip" from baseline (a straight line drawn between the RPE and the outer segment tip portions of the profile) was measured so the magnitude of the hyporeflective band signal intensity was considered undetectable, a result that agreed with prior data collected from male S6 mice.[29,33] For completeness, we present the thicknesses of the other retinal layers between light and dark conditions (Supplementary Figs. S4 and S5).

Electron Microscopy Evaluation of Rod Inner Segment Ellipsoid Mitochondria Numbers

A difference in rod inner segment ellipsoid mitochondria distribution was detected between B6J mice that had been dark-adapted and those exposed to one hour of light (Fig. 5). Dark-adapted mice had a significantly greater number of mitochondria within the distal IS, whereas one hour of light exposure led to more mitochondria in the proximal IS. In contrast, S6 mice did not show a difference in distal, mid, and proximal inner segment ellipsoid mitochondria numbers between dark and light conditions (Fig. 5). Furthermore, in distal and proximal inner segment ellipsoid, there are more mitochondria in S6 than in B6J mice in light and dark (Fig. 5). The width of inner segment ellipsoid mitochondria was also compared from dark and light B6J and S6 mice; no strain difference in the ratio of dark to light values was found (B6J, 1.022 [0.929–1.124]; S6, 0.988 [0.898–1.086]; mean [95% lower confidence interval (LCI)–95% upper confidence interval (UCI)]).

Discussion

In this study, dark-light changes in the OCT rod ISez profile shape (as measured by the aspect ratio) are reported for the first time. Our data indicate a change in shape of the ISez that was correlated with rod energy demand. First, the higher energy configuration expected for dark-adapted B6J mice showed a greater ISez aspect ratio whereas the lower energy configuration of the light-adapted B6J mice showed a smaller ISez AR.[18–20,66] Second, the different ISez aspect ratio for light-adapted B6J and S6 mice mirrored the reported strain-dependent differences in mitochondrial activity and injury vulnerability detailed in several publications (Fig. 3).[29,30,32,33,49] As a consequence of the higher ISez aspect ratio in light-adapted S6 mice, no dark-light changes in ISez aspect ratio were found. Third, S6 rod inner segment ellipsoid contained more mitochondria than that in B6J mice, as measured by EM, a finding that was reflected in the OCT ISez aspect ratio (Figs. 2 and 5). In this initial study, only male S6 mice were studied because no evidence was noted for a sex difference in the functional ISez aspect ratio response in B6J mice. In this study, we introduce the aspect ratio as a useful approach for characterizing functional changes in the ISez profile shape; more work is needed to determine whether the aspect ratio is an optimal shape descriptor of the ISez profile.

The spatial distribution of mitochondria is linked to its ability to meet a cells energy needs although it may not be the only factor.[67,68] For example, factors such as the number of mitochondria–plasma membrane contacts between adjacent photoreceptor cells likely also contribute to this goal.[69] To help interpret the B6J versus S6 differences in functional ISez aspect ratio response in terms of rod bioenergetics, we evaluated two other energy-dependent OCT

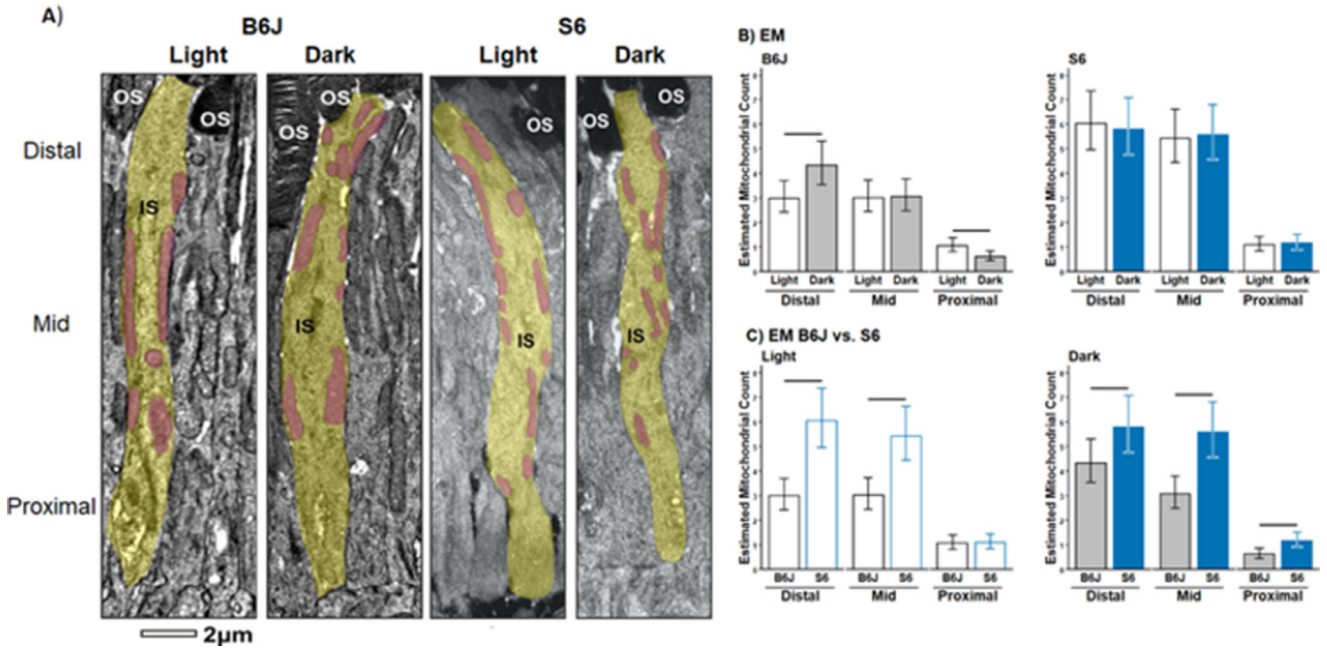

Figure 5. B6J versus S6 mice rod inner segment ellipsoid mitochondria distribution and number measured by EM. (**A**) Electron microscopy images of representative rod inner segment ellipsoid (*yellow*) and mitochondria (*purple*) in one-hour light versus dark B6J (*left two panels*) versus S6 (*right two panels*) mice. The distal inner segment ellipsoid is identified by the presence of outer segments (OS). (**B**) Quantification of mitochondrial number within each third region-of-interest within the inner segment ellipsoid in light versus dark (*top row*) and between B6J (*black bars*) and S6 (*blue bars*) mice for each light condition (*bottom row*). *Horizontal black line*: $P < 0.05$, 95% confidence interval measured from light ($n = 3$/strain), dark ($n = 3$/strain), 15 inner segment ellipsoid/mouse/strain.

biomarkers in the outer retina, namely the ELM-RPE thickness and magnitude of the hyporeflective band signal intensity between the photoreceptor tips and apical RPE.[21,33] In the dark the ELM-RPE is thinner than in the light.[20,24–26] The signaling pathway regulating this physiology is well established.[22,23,30,64,70,71] Briefly, with dark-adaptation, rod cGMP accumulates in the outer segment to maintain persistently open cyclic nucleotide-gated channels, an event that depolarizes the rod membrane and increases ion pumping/mitochondrial energy use for the dark current compared to light-adaptation.[22–28] Increased mitochondrial activity in the dark also produces more lactate, CO_2, and waste water, which acidifies the subretinal space and triggers an increase in apical RPE co-transporter–based water removal with concomitant shrinkage of the ELM-RPE region.[21] Our other biomarker, the magnitude of the hyporeflective band signal intensity, also decreases in the dark compared to the light and is correlated with ELM-RPE changes, but unlike the ELM-RPE, the magnitude of the hyporeflective band signal intensity was pH independent.[33]

In B6J mice, in the dark/light, we found a larger/smaller ISez aspect ratio, respectively, together with associated thinner/thicker ELM-RPE and smaller/larger magnitude of the hyporeflective band signal intensity. When our three biomarker results are considered together, they are consistent with a higher energy state in the dark and a lower energy state in the light. In contrast, the retina of S6 mice, which are reported to operate at a higher mitochondria efficacy relative to that in B6J mice, showed rod ISez aspect ratio's that were similarly high in dark and light, with a smaller ELM-RPE thickness difference.[29,33,48–50,72] These data underscore the usefulness of measuring the ISez aspect ratio together with ELM-RPE thickness and magnitude of the hyporeflective band signal intensity in wildtype mice for evaluating the rod energy-landscape. Further testing of the usefulness of our three biomarkers in disease models in ongoing.

Here, we also began to test whether changes in rod ISez aspect ratio reflect the spatial distribution of the rod inner segment ellipsoid mitochondria, which can scatter light and act as a source of OCT reflectivity.[52,55] First-time evidence was found that the number of mitochondria within different thirds of the rod inner segment ellipsoid change as a function of dark-light conditions in B6J but not S6 mice (Fig. 5). These data suggest movement of mitochondria toward the distal inner segment ellipsoid under high energy demand conditions in B6J mice as a potential compensatory mechanism for its less efficient mitochondria compared to that in S6 mice.[29,30,32,33,49] Intriguingly, the greater number of rod inner segment ellipsoid mitochondria in S6 versus B6J mice is in-line with the higher OCT ISez aspect ratio values in light-adapted S6 versus B6J mice (Fig. 2). Further studies are warranted into rod mitochondria dynamics within the inner segment ellipsoid and their link to the OCT ISez aspect ratio because impairment in mitochondria spatial rearrangements are believed to play a pathogenic role in the development of neurodegenerative diseases of rod photoreceptors.[73–76]

In future studies, the addition of other in vivo biomarkers may further clarify how well the inner segment ellipsoid mitochondria are performing.[18,30,77] For example, it is possible to evaluate mitochondria activity based on a proxy for the production of free radicals from rod mitochondria in this region.[78] Free radicals are inherently paramagnetic, and their production can be monitored by measuring the MRI spin-lattice relaxation rate (R1 [=1/T1]) from the ISez (calibrated against OCT) in vivo during dark and light conditions.[50,79] R1 MRI can also map rod ISez mitochondria oxidative stress, an important component of the energy-

landscape, by comparing localized R1 values obtained before and after administration of antioxidants (i.e., a QUEST protocol) in dark versus light conditions.[48,80] Also, evaluating ex vivo biomarkers, such as oxygen consumption rate, can provide further insight into the health of the rod mitochondria.[18,30,77]

In summary, this study identifies, for the first time, energy-dependent changes in the ISez shape profile and inner segment ellipsoid mitochondria distribution noted on EM. These results support future studies of the OCT-based rod ISez aspect ratio as a novel biomarker of mitochondria correlated to its activity (e.g., its dynamics and oxygen consumption rate). We anticipate that the shape of the ISez may also be a useful proxy of the cone energy-landscape, in, for example, the human fovea. This might be possible because in zebrafish, the cone inner segment ellipsoid shows a change in the spatial distribution of mitochondria with dark-light conditions.[81] Also, in humans, cone mitochondria can shrink, as well as translocate, during age-related macular degeneration, a disease suggested to have an important contribution from mitochondria.[55,82] In any event, more work is also needed on the image analysis-side (e.g., deriving ISez shape profiles from log vs. linear-based images, and whether normalization is needed), as well as on the physiology side (e.g., whether ISez changes with time of day, anesthesia, length of light exposure, aging, disease, and treatment).[29,30,32,33,49] The results of this study raise the possibility of future application of rod ISez profile shape to evaluate inner segment ellipsoid mitochondria activity in vivo in mitochondria-based diseases of the retina, such as diabetic retinopathy, as well as in primary mitochondria morbidities, such as Alzheimer's disease.[82,83]

Acknowledgments

The authors thank Matt Hayes at UCL Institute of Ophthalmology for preparing some of the samples for EM.

Disclosure: **B.A. Berkowitz,** None; **R.H. Podolsky,** None; **K.L. Childers,** None; **T. Burgoyne,** None; **G. De Rossi,** None; **H. Qian,** None; **R. Roberts,** None; **R. Katz,** None; **R. Waseem,** None; **C. Goodman,** None

References

1. Perron NR, Beeson C, Rohrer B. Early alterations in mitochondrial reserve capacity; a means to predict subsequent photoreceptor cell death. *J Bioenerg Biomembr*. 2013;45:101–109.
2. Gopalakrishnan S, Mehrvar S, Maleki S, et al. Photobiomodulation preserves mitochondrial redox state and is retinoprotective in a rodent model of retinitis pigmentosa. *Sci Rep*. 2020;10:1–13.
3. Ozaki T, Ishiguro S-i, Hirano S, et al. Inhibitory peptide of mitochondrial -calpain protects against photoreceptor degeneration in rhodopsin transgenic S334ter and P23H rats. *PloS One*. 2013;8:e71650–e71650.
4. Xu L, Kong L, Wang J, Ash JD. Stimulation of AMPK prevents degeneration of photoreceptors and the retinal pigment epithelium. *Proc Natl Acad Sci USA*. 2018;115:10475–10480.
5. Wang T, Reingruber J, Woodruff ML, et al. The PDE6 mutation in the rd10 retinal degeneration mouse model causes protein mislocalization and instability and promotes cell death through increased ion influx. *J Biol Chem*. 2018;293:15332–15346.
6. Nakazawa M, Suzuki Y, Ito T, Metoki T, Kudo T, Ohguro H. Long-term effects of nilvadipine against progression of the central visual field defect in retinitis pigmentosa: an extended study. *Biomed Res Int*. 2013;2013:585729–585729.
7. Nakazawa M, Ohguro H, Takeuchi K, Miyagawa Y, Ito T, Metoki T. Effect of nilvadipine on central visual field in retinitis pigmentosa: a 30-month clinical trial. *Ophthalmologica*. 2011;225:120–126.
8. Yamazaki H, Ohguro H, Maeda T, et al. Preservation of retinal morphology and functions in royal college surgeons rat by nilvadipine, a Ca(2+) antagonist. *Invest Ophthalmol Vis Sci*. 2002;43:919–926.
9. Porto FB, Mack G, Sterboul MJ, et al. Isolated late-onset cone-rod dystrophy revealing a familial neurogenic muscle weakness, ataxia, and retinitis pigmentosa syndrome with the T8993G mitochondrial mutation. *Am J Ophthalmol*. 2001;132:935–937.
10. Kutsyr O, Sánchez-Sáez X, Martínez-Gil N, et al. Gradual increase in environmental light intensity induces oxidative stress and inflammation and accelerates retinal neurodegeneration. *Invest Ophthalmol Vis Sci*. 2020;61:1.
11. Berkowitz BA. Preventing diabetic retinopathy by mitigating subretinal space oxidative stress in vivo. *Vis Neurosci*. 2020;37:E002.
12. Berkowitz BA, Bissig D, Roberts R. MRI of rod cell compartment-specific function in disease and treatment in vivo. *Prog Retin Eye Res*. 2016;51:90–106.
13. Yokomizo H, Maeda Y, Park K, et al. Retinol binding protein 3 is increased in the retina of patients with diabetes resistant to diabetic retinopathy. *Sci Transl Med*. 2019;11 (499):eaau6627.
14. Shinhmar H, Grewal M, Sivaprasad S, et al. Optically Improved Mitochondrial Function Redeems Aged Human Visual Decline. *J Gerontol A Biol Sci Med Sci*. 2020;75:e49–e52.
15. Alam NM, Douglas RM, Prusky GT. Treatment of age-related visual impairment with a peptide acting on mitochondria. *Dis Models Mech*. 2022;15:dmm048256.
16. Gkotsi D, Begum R, Salt T, et al. Recharging mitochondrial batteries in old eyes. Near infra-red increases ATP. *Exp Eye Res*. 2014;122:50–53.
17. Linsenmeier RA. Effects of light and darkness on oxygen distribution and consumption in the cat retina. *J Gen Physiol*. 1986;88:521–542.
18. Medrano CJ, Fox DA. Oxygen consumption in the rat outer and inner retina: light- and pharmacologically-induced inhibition. *Exp Eye Res*. 1995;61:273–284.
19. Okawa H, Sampath AP, Laughlin SB, Fain GL. ATP Consumption by Mammalian Rod Photoreceptors in Darkness and in Light. *Curr Biol*. 2008;18:1917–1921.
20. Linton JD, Holzhausen LC, Babai N, et al. Flow of energy in the outer retina in darkness and in light. *Proc Natl Acad Sci USA*. 2010;107:8599–8604.
21. Berkowitz BA, Qian H. OCT imaging of rod mitochondrial respiration in vivo. *Exp Biol Med (Maywood)*. 2021;15353702211013799.
22. Bissig D, Berkowitz BA. Light-dependent changes in outer retinal water diffusion in rats in vivo. *Mol Vis*. 2012;18:2561–2562.xxx.
23. Berkowitz BA, Grady EM, Khetarpal N, Patel A, Roberts R. Oxidative stress and light-evoked responses of the posterior segment in a mouse model of diabetic retinopathy. *Invest Ophthalmol Vis Sci*. 2015;56:606–615.
24. Adijanto J, Banzon T, Jalickee S, Wang NS, Miller SS. CO2-induced ion and fluid transport in human retinal pigment epithelium. *J Gen Physiol*. 2009;133:603–622.
25. Berkowitz BA, Bissig D, Roberts R. MRI of rod cell compartment-specific function in disease and treatment invivo. *Prog Retin Eye Res*. 2016;51:90–106.
26. Hamann S, Kiilgaard JF, la Cour M, Prause JU, Zeuthen T. Cotransport of H+, lactate, and H2O in porcine retinal

pigment epithelial cells. *Exp Eye Res*. 2003;76:493–504.
27. Li Y, Fariss RN, Qian JW, Cohen ED, Qian H. Light-Induced Thickening of Photoreceptor Outer Segment Layer Detected by Ultra-High Resolution OCT Imaging. *Invest Ophthalmol Vis Sci*. 2016;57:OCT105–OCT111.
28. Lu CD, Lee B, Schottenhamml J, Maier A, Pugh EN, Fujimoto JG. Photoreceptor layer thickness changes during dark adaptation observed with ultrahigh-resolution optical coherence tomography. *Invest Ophthalmol Vis Sci*. 2017;58:4632–4643.
29. Berkowitz BA, Olds HK, Richards C, et al. Novel imaging biomarkers for mapping the impact of mild mitochondrial uncoupling in the outer retina in vivo. *PLOS ONE*. 2020;15:e0226840.
30. Berkowitz BA, Podolsky RH, Qian H, et al. Mitochondrial respiration in outer retina contributes to light-evoked increase in hydration in vivo. *Invest Ophthalmol Vis Sci*. 2018;59:5957–5964.
31. Li Y, Zhang Y, Chen S, Vernon G, Wong WT, Qian H. Light-dependent OCT structure changes in photoreceptor degenerative rd 10 mouse retina. *Invest Ophthalmol Vis Sci*. 2018;59:1084–1094.
32. Berkowitz BA, Podolsky RH, Lins-Childers KM, Li Y, Qian H. Outer retinal oxidative stress measured in vivo using QUEnch-assiSTed (QUEST) OCT. *Invest Ophthalmol Vis Sci*. 2019;60:1566–1570.
33. Gao S, Li Y, Bissig D, et al. Functional regulation of an outer retina hyporeflective band on optical coherence tomography images. *Sci Rep*. 2021;11:10260.
34. Kanwar M, Chan PS, Kern TS, Kowluru RA. Oxidative damage in the retinal mitochondria of diabetic mice: possible protection by superoxide dismutase. *Invest Ophthalmol Vis Sci*. 2007;48:3805–3811.
35. Duraisamy AJ, Mohammad G, Kowluru RA. Mitochondrial fusion and maintenance of mitochondrial homeostasis in diabetic retinopathy. *Biochim Biophys Acta Mol Basis Dis*. 2019;1865:1617–1626.
36. Bisbach CM, Hass DT, Robbings BM, et al. Succinate Can shuttle reducing power from the hypoxic retina to the O(2)-rich pigment epithelium. *Cell Rep*. 2020;31:107606.
37. Tarchick MJ, Cutler AH, Trobenter TD, et al. Endogenous insulin signaling in the RPE contributes to the maintenance of rod photoreceptor function in diabetes. *Exp Eye Res*. 2019;180:63–74.
38. Keeling E, Chatelet DS, Tan NY, et al. 3D-reconstructed retinal pigment epithelial cells provide insights into the anatomy of the outer retina. *Int J Mol Sci*. 2020;21:8408.
39. Spaide RF, Curcio CA. Anatomical correlates to the bands seen in the outer retina by optical coherence tomography: literature review and model. *Retina*. 2011;31:1609–1619.
40. Lee KE, Heitkotter H, Carroll J. Challenges associated with ellipsoid zone intensity measurements using optical coherence tomography. *Transl Vis Sci Technol*. 2021;10:27.
41. Perkins GA, Ellisman MH, Fox DA. Three-dimensional analysis of mouse rod and cone mitochondrial cristae architecture: bioenergetic and functional implications. *Mol Vis*. 2003;9:60–73.
42. Fox DA, Poblenz AT, He L. Calcium overload triggers rod photoreceptor apoptotic cell death in chemical-induced and inherited retinal degenerations. *Ann N Y Acad Sci*. 1999;893:282–285.
43. Schaal KB, Rosenfeld PJ. The controversy of band# 2. *Retina Specialist*. 2018. Available at https://www.retina-specialist.com/article/the-controversy-of-band-2. Accessed March, 2022.
44. Cai CX, Locke KG, Ramachandran R, Birch DG, Hood DC. A comparison of progressive loss of the ellipsoid zone (EZ) band in autosomal dominant and x-linked retinitis pigmentosa. *Invest Ophthalmol Vis Sci*. 2014;55:7417–7422.
45. Jonnal RS, Kocaoglu OP, Zawadzki RJ, Lee S-H, Werner JS, Miller DT. The cellular origins of the outer retinal bands in optical coherence tomography images. *Invest Ophthalmol Vis Sci*. 2014;55:7904–7918.
46. Staurenghi G, Sadda S, Chakravarthy U, Spaide RF. Proposed lexicon for anatomic landmarks in normal posterior segment spectral-domain optical coherence tomography: the IN•OCT consensus. *Ophthalmology*. 2014;121:1572–1578.
47. Ronchi JA, Figueira TR, Ravagnani FG, Oliveira HC, Vercesi AE, Castilho RF. A spontaneous mutation in the nicotinamide nucleotide transhydrogenase gene of C57BL/6J mice results in mitochondrial redox abnormalities. *Free Radic Biol Med*. 2013;63:446–456.
48. BerkowitzBA, Podolsky RH, Farrell B, et al. D-cis-Diltiazem can produce oxidative stress in healthy depolarized rods in vivo. *Invest Ophthalmol Vis Sci*. 2018;59:2999–3010.
49. Berkowitz BA, Podolsky RH, Lenning J, et al. Sodium Iodate Produces a Strain-Dependent Retinal Oxidative Stress Response Measured In Vivo Using QUEST MRI. *Invest Ophthalmol Vis Sci*. 2017;58:3286–3293.
50. Berkowitz BA, Bredell BX, Davis C, Samardzija M, Grimm C, Roberts R. Measuring in vivo free radical production by the outer retina. *Invest Ophthalmol Vis Sci*. 2015;56:7931–7938.
51. Jeon CJ, Strettoi E, Masland RH. The major cell populations of the mouse retina. *J Neurosci*. 1998;18:8936–8946.
52. Beauvoit B, Evans SM, Jenkins TW, Miller EE, Chance B. Correlation between the light scattering and the mitochondrial content of normal tissues and transplantable rodent tumors. *Anal Biochem*. 1995;226:167–174.
53. Kam JH, Jeffery G. To unite or divide: mitochondrial dynamics in the murine outer retina that preceded age related photoreceptor loss. *Oncotarget*. 2015;6:26690–26701.
54. Litts KM, Zhang Y, Freund KB, Curcio CA. Optical coherence tomography and histology of age-related macular degeneration support mitochondria as reflectivity sources. *Retina*. 2018;38:445–461.
55. Litts KM, Messinger JD, Freund KB, Zhang Y, Curcio CA. Inner segment remodeling and mitochondrial translocation in cone photoreceptors in age-related macular degeneration with outer retinal tubulation. *Invest Ophthalmol Vis Sci*. 2015;56:2243–2253.
56. Schneider CA, Rasband WS, Eliceiri KW. NIH Image to ImageJ: 25 years of image analysis. *Nature Methods*. 2012;9:671–675.
57. DeRamus ML, Stacks DA, Zhang Y, Huisingh CE, McGwin G, Pittler SJ. GARP2 accelerates retinal degeneration in rod cGMP-gated cation channel β-subunit knockout mice. *Sci Rep*. 2017;7:42545.
58. Soukup P, Maloca P, Altmann B, Festag M, Atzpodien EA, Pot S. Interspecies Variation of Outer Retina and Choriocapillaris Imaged With Optical Coherence Tomography. *Invest Ophthalmol Vis Sci*. 2019;60:3332–3342.
59. Zhang T, Kho AM, Yiu G, Srinivasan VJ. Visible Light Optical Coherence Tomography (OCT) Quantifies Subcellular Contributions to Outer Retinal Band 4. *Transl Vis Sci Technol*. 2021;10:30–30.
60. Berkowitz BA, Podolsky RH, Childers KL, et al. Rod Photoreceptor Neuroprotection in Dark-Reared Pde6brd10 Mice. *Invest Ophthalmol Vis Sci*. 2020;61:14–14.
61. Burgoyne T, Meschede IP, Burden JJ, Bailly M, Seabra MC, Futter CE. Rod disc renewal occurs by evagination of the ciliary plasma membrane that makes cadherin-based contacts with the inner segment. *Proc Natl Acad Sci USA*. 2015;112:15922–15927.

Investigative Ophthalmology & Visual Science

62. Russell MR, Lerner TR, Burden JJ, et al. 3D correlative light and electron microscopy of cultured cells using serial blockface scanning electron microscopy. *J Cell Sci*. 2017;130:278–291.
63. Ohta K, Hirashima S, Miyazono Y, Togo A, Nakamura K-i. Correlation of organelle dynamics between light microscopic live imaging and electron microscopic 3D architecture using FIB-SEM. *Microscopy*. 2021;70:161–170.
64. Li JD, Govardovskii VI, Steinberg RH. Light-dependent hydration of the space surrounding photoreceptors in the cat retina. *Vis Neurosci*. 1994;11:743–752.
65. Berkowitz BA, Grady EM, Khetarpal N, Patel A, Roberts R. Oxidative stress and light-evoked responses of the posterior segment in a mouse model of diabetic retinopathy. *Invest Ophthalmol Vis Sci*. 2015;56:606–615.
66. Braun RD, Linsenmeier RA, Goldstick TK. Oxygen consumption in the inner and outer retina of the cat. *Invest Ophthalmol Vis Sci*. 1995;36:542–554.
67. Seager R, Lee L, Henley JM, Wilkinson KA. Mechanisms and roles of mitochondrial localisation and dynamics in neuronal function. *Neuronal Signal*. 2020;4:Ns20200008.
68. Sun N, Finkel T. Cardiac mitochondria: a surprise about size. *J Mol Cell Ccardiol*. 2015;82:213–215.
69. Meschede IP, Ovenden NC, Seabra MC, et al. Symmetric arrangement of mitochondria:plasma membrane contacts between adjacent photoreceptor cells regulated by Opa1. *Proc Natl Acad Sci USA*. 2020;117:15684–15693.
70. Govardovskii VI, Li JD, Dmitriev AV, Steinberg RH. Mathematical model of TMA+ diffusion and prediction of light-dependent subretinal hydration in chick retina. *Invest Ophthalmol Vis Sci*. 1994;35:2712–2724.
71. Huang B, Karwoski CJ. Light-evoked expansion of subretinal space volume in the retina of the frog. *J Neurosci*. 1992;12:4243–4252.
72. Berkowitz BA. Mitochondrial respiration in outer retina contributes to light-evoked increase in hydration in vivo. *Invest Ophthalmol Vis Sci*. 2018;59:5957–5964.
73. Gopalakrishnan S, Mehrvar S, Maleki S, et al. Photobiomodulation preserves mitochondrial redox state and is retinoprotective in a rodent model of retinitis pigmentosa. *Sci Rep*. 2020;10:20382.
74. Roberts R. Sodium iodate produces a strain-dependent retinal oxidative stress response measured in vivo using QUEST MRI. *FASEB J*. 2017;58:3286–3293.
75. Cooper LL, Hansen RM, Darras BT, et al. Rod photoreceptor function in children with mitochondrial disorders. *Arch Ophthal*. 2002;120:1055–1062.
76. He L, Poblenz AT, Medrano CJ, Fox DA. Lead and calcium produce rod photoreceptor cell apoptosis by opening the mitochondrial permeability transition pore. *J Biol Chem*. 2000;275:12175–12184.
77. Kanow MA, Giarmarco MM, Jankowski CS, et al. Biochemical adaptations of the retina and retinal pigment epithelium support a metabolic ecosystem in the vertebrate eye. *Elife*. 2017;6:e28899.
78. Murphy MP. How mitochondria produce reactive oxygen species. *Biochem J*. 2009;417:1–13.
79. Berkowitz BA, Lewin AS, Biswal MR, Bredell BX, Davis C, Roberts R. MRI of Retinal Free Radical Production With Laminar Resolution In Vivo. *Invest Ophthalmol Vis Sci*. 2016;57:577–585.
80. Berkowitz BA. Oxidative stress measured in vivo without an exogenous contrast agent using QUEST MRI. *J Magn Reson*. 2018;291:94–100.
81. Giarmarco MM, Brock DC, Robbings BM, et al. Daily mitochondrial dynamics in cone photoreceptors. *Proc Natl Acad Sci USA*. 2020;117:28816–28827.
82. Ferrington DA, Fisher CR, Kowluru RA. Mitochondrial Defects Drive Degenerative Retinal Diseases. *Trends Mol Med*. 2020;26:105–118.
83. Weidling IW, Swerdlow RH. Mitochondria in Alzheimer's disease and their potential role in Alzheimer's proteostasis. *Exp Neurol*. 2020;330:113321.

Investigative Ophthalmology & Visual Science